

PAPER

Linear polarization of anisotropically excited x-ray lines from the $n = 2$ complex in He-like Ar^{16+}

To cite this article: Dipti *et al* 2020 *J. Phys. B: At. Mol. Opt. Phys.* **53** 115701

View the [article online](#) for updates and enhancements.

Recent citations

- [Measurements of linear polarization of satellite transitions from Li- and Be-like Ar ions](#)
A C Gall *et al*



IOP | ebooks™

Bringing together innovative digital publishing with leading authors from the global scientific community.

Start exploring the collection—download the first chapter of every title for free.

Linear polarization of anisotropically excited x-ray lines from the $n = 2$ complex in He-like Ar^{16+}

Dipti^{1,4} , S W Buechele^{1,2}, A C Gall^{1,2} , S Sanders^{1,2}, C I Szabo^{1,3} ,
R Silwal^{1,2}, E Takacs^{1,2}  and Yu Ralchenko^{1,4} 

¹ National Institute of Standards and Technology, Gaithersburg, MD 20899, United States of America

² Department of Physics and Astronomy, Clemson University, Clemson, SC 29634, United States of America

³ Theiss Research, 7411 Eads Ave, La Jolla, CA 92037, United States of America

E-mail: fnu.dipti@nist.gov and yuri.ralchenko@nist.gov

Received 6 December 2019, revised 13 January 2020

Accepted for publication 5 March 2020

Published 13 May 2020



Abstract

High-resolution x-ray spectra were recorded at the National Institute of Standards and Technology electron beam ion trap (EBIT) using two Johann-type crystal spectrometers, with their dispersion planes oriented parallel and perpendicular to the beam direction. The linear polarizations of the $1s^2 - 1s2l$ transitions in He-like argon ions were determined from the measured spectra at electron beam energies of 3.87 and 7.91 keV. The theoretical analysis was performed using detailed collisional-radiative modeling of the non-Maxwellian EBIT plasma with the NOMAD code modified to account for magnetic sublevel atomic kinetics. Effects influencing the polarizations of the observed $1s^2 - 1s2l$ lines were investigated, including radiative cascades, the $1s^2\ ^1S_0 - 1s2s\ ^1S_0$ two-photon transition, and the charge exchange recombination of H-like argon ions. With these included, the measured polarizations of the resonance ($1s^2\ ^1S_0 - 1s2p\ ^1P_1$), intercombination ($1s^2\ ^1S_0 - 1s2p\ ^3P_1$), and forbidden lines ($1s^2\ ^1S_0 - 1s2s\ ^3S_1$, $1s^2\ ^1S_0 - 1s2p\ ^3P_2$) were found to be in good agreement with the calculations.

Keywords: polarization, spectroscopy, highly-charged ions, electron beam ion trap, magnetic sublevels, collisional-radiative modeling

(Some figures may appear in colour only in the online journal)

1. Introduction

Abundant in hot plasmas, highly-charged ions generally emit isotropic and unpolarized radiation due to the isotropic velocity distribution of the plasma electrons. In cases, however, where anisotropic electron distributions are present, plasma sources can produce polarized emissions [1] that affect the measured line intensities and therefore must be taken into account when inferring physical information from the spectral features. This can be relevant both in astrophysical sources such as solar flares [2], neutron stars [3], and supernova remnants [4], and in laboratory settings, such as electron beam ion traps (EBITs) and laser-excited plasmas [5].

The unidirectional quasi-monoenergetic electron beam of the EBIT and the charge-state selectivity of the device, when combined with polarization sensitive spectrometers, provide an ideal setup for polarization studies of atomic processes of hot plasmas. In fact, one of the first measurements ever reported using an EBIT device demonstrated that the polarization of He-like Sc^{19+} x-ray lines are affected by the hyperfine interaction [6]. This was followed by an EBIT measurement of the polarization of K_β lines in He-like V^{21+} , also found to be sensitive to the hyperfine interaction [7].

As the He-like $1s^2\ ^1S_0 - 1s2p\ ^1P_1$ resonance (w), $1s^2\ ^1S_0 - 1s2s\ ^3S_1$ (z) and $1s^2\ ^1S_0 - 1s2p\ ^3P_2$ (x) forbidden and $1s^2\ ^1S_0 - 1s2p\ ^3P_1$ intercombination (y) lines are often used for density and temperature diagnostics of hot plasmas, with the region of sensitivity depending on the nuclear charge Z

⁴ Authors to whom any correspondence should be addressed.

[8], several polarization measurements have been reported along the isoelectronic sequence from EBITs. These include measurements of Ti^{20+} [9] and the astrophysically relevant Fe^{24+} [10, 11] ions. These measurements also reported the polarizations of lines from the neighboring Li-like Ti^{19+} [9] and Fe^{23+} [11] charge states, and more recent measurements have expanded upon this set to include lines from H-like Ti^{21+} [12], Fe^{25+} and Ar^{17+} [13] ions. Similar to the He-like Fe and Ti studies, EBIT measurements of He-like Mg^{10+} [14] (excited near the excitation threshold of the strong resonance line) were reported in a study of the cyclotron motion of the electrons in the EBIT electron beam.

To better understand the dependence of the polarization on the electron beam energy, He-like and Li-like resonance lines in S^{14+} and S^{13+} [15] were measured over a broad range of beam energies. Similarly, in an early experiment at the National Institute of Standards and Technology (NIST) EBIT, the electron beam energy dependence of the polarization of a magnetic quadrupole (M2) x-ray transition in Ne-like Ba^{46+} was studied using two Johann-type bent crystal spectrometers oriented perpendicular to each other relative to the electron beam direction [16]. An analogous detector setup was used to measure emission from Ar^{16+} at the Torus Experiment of Technology Oriented Research (TEXTOR-94), where the w , x , y , and z lines were found to be unpolarized for two ohmic experimental conditions [17]. Later, the polarizations of the resonance and intercombination lines were inferred from the ratio of the two lines measured from an Ar Z-pinch plasma with two crystal analyzers employing position sensitive x-ray films to record the spectra [18].

On the theoretical side, the polarization dependent x-ray spectra of Ly_α satellites in laser produced Si plasma [19] as well as K_α lines of He-like Fe ion produced in an EBIT [20] were analyzed using a collisional-radiative (CR) model. The polarization of x-ray lines following electron-impact excitation in H-like and He-like ions were reported using different computational approaches such as relativistic distorted-wave [21–26], relativistic convergent close-coupling [27], and semi-relativistic R-matrix [28] theories. Effects of the Breit [22] and the hyperfine interaction [29] on the polarization of x-ray lines were also studied for He-like ions.

The polarization of x-ray emission was never measured for He-like Ar ions in the EBIT. In this work we report the He-like EBIT measurements by employing the same spectrometer setup used in the early NIST work [16], utilizing advanced x-ray charge-coupled device (CCD) detectors to accurately determine the polarizations of He-like Ar^{16+} transitions at two electron beam energies. One of the goals is to provide the benchmark data through a well-controlled experiment for validation of different theoretical approaches. In the following sections we outline the details of the experiment, the processing and analysis of CCD detector data, and the experimental determination of the line polarization. Detailed theoretical analysis of the polarization of the He-like lines is then discussed including the effects of the $1s^2\ ^1\text{S}_0 - 1s2s\ ^1\text{S}_0$ two-photon transition, radiative recombination (RR), and charge exchange (CX). Our theoretical calculations are based on the magnetic sublevel CR NOMAD [30] model aided by atomic data from the flexible atomic code (FAC) [31].

Comparison of our experimental and theoretical polarization results is presented at two different electron beam energies: above the threshold excitation energy for these transitions, and above the ionization potential for the He-like charge state.

2. Experiment

The experiment was performed at the NIST EBIT facility in Gaithersburg, Maryland. The operation of the NIST EBIT has been described in detail in earlier papers (see for example [32]). To summarize, the EBIT operates with a quasi-mono-energetic electron beam of up to a 150 mA current. A strong 2.7 T magnetic field compresses the electron beam to about a $70\ \mu\text{m}$ diameter and $10^{11}\ \text{cm}^{-3}$ density in the trap. The beam is accelerated from a Pierce type electron gun at ground potential towards the trap region by applying up to 30 kV voltage to a series of three drift tube electrodes in the center of the machine. Neutral atoms or low-charged ions can be injected into the trap [33, 34] to interact with the electron beam. Trapped ions are stripped to higher-charged states through electron-impact ionization. Ions become radially confined by both the space charge of the electron beam and the magnetic field present in the drift tube region and axially by a bias voltage on the outer drift tubes and the space charge potential difference due to their geometric structure.

The EBIT parameters for this measurement are detailed in table 1. The trapping drift tube voltage was set to 4.0 and 8.0 kV in a steady state mode, where the voltage is held constant during the measurement. These beam energies were chosen in order to optimize for the production of He-like Ar ions inside the trap, to avoid any resonant process such as dielectronic recombination (DR), and to cover the two theoretically interesting regions explained in the introduction. The drift tube voltage was cycled every 5 s to displace any trapped contaminants, such as barium dispensed from the cathode surface of the electron gun. At the end of the 5 s cycle the middle drift tube voltage was raised for about 10 ms to displace ions towards the collector. The EBIT experimental parameters, including the gas injection pressure, were optimized to maximize the x-ray count rate recorded by a high purity solid state Ge detector.

The electron energy distribution function (EEDF) in the EBIT is assumed to have a Gaussian profile, where the full width at half maximum (FWHM) was experimentally determined by measuring the intensity variation of the well separated, satellite j line (Gabriel notation [8]) from Li-like Ar as a function of the electron beam energy. The beam energy was finely scanned across the satellite at 2.22 keV in 10 eV steps. From the theoretical and experimental resonance energy for this line, the estimated space-charge corrected electron beam energies (see, e.g. [35]) are 3.87 keV and 7.91 keV for the 4.0 kV and 8.0 kV trap settings respectively. The 3.87 keV energy is about 730 eV above the excitation energy of the resonance (w) line, well above the ionization energy of Li-like Ar (918.375 eV), and below the ionization energy for He-like Ar ions (4120.67 eV) in the ground state (values from the NIST Atomic Spectra Database [36]). The beam energy of 7.91 keV is above the ionization energy of H-like Ar,

Table 1. Operational parameters of the NIST EBIT in the current experiment.

Parameter	Value
Electron beam current	128 mA
Drift tube voltage	4.0 and 8.0 kV
Dump cycle	5 s
Pressure of gas injector	5.1×10^{-3} Pa
Trap length	2 cm
Magnetic field	2.7 T
Full width at half maximum (FWHM)	≈ 40 eV

therefore the charge state distribution is expected to be drastically different from that at 3.87 keV. Data were collected in three minute intervals at each electron beam energy, for total live data acquisition times of 39 min and 42 min at 3.87 keV and 7.91 keV respectively.

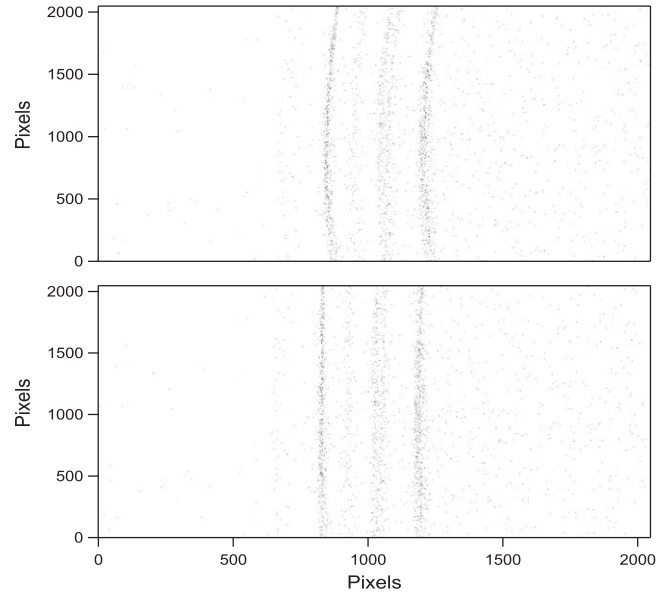
Two Johann-type cylindrically curved Bragg crystal spectrometers equipped with CCD detectors were used to disperse and observe x-rays. The high resolution spectrometers are able to resolve features which are less than 2 eV apart at around 3 keV x-ray energy. Both spectrometers were equipped with Si(111) crystals, with an interplanar distance of 3.135 Å [37]. The dispersion plane of one of the crystals was oriented parallel to the direction of the electron beam, while the second crystal was oriented such that the dispersion plane was perpendicular to the beam. These are hereafter referred to as vertical and horizontal spectrometer orientations, respectively. During our measurements, the spectrometers were set with a central Bragg angle of 39° such that the He-like emission features were centered within the approximately 120 eV spectral bandwidth.

3. Data analysis

3.1. Processing raw data

The signal collected by the 2048×2048 CCD pixel arrays included contributions from dispersed x-rays, electronic and readout noises, and cosmic rays. The majority of the background noise was filtered out during the initial processing of the CCD data using energy discrimination techniques, while cosmic rays were eliminated using spatial filters for streak size and intensity as described by Hudson *et al* [38].

While both spectrometers used in the experiment have curved crystals that focus x-rays onto a focusing (Rowland) circle [39], the two orientations see different source geometry. As a result, the vertical spectrometer incurs significant aberrations in the form of drastic curvature of the spectral lines [40]. This aberration was corrected by fitting a polynomial to the curvature at each column of pixels, and shifting the matrix of the spectral intensity correspondingly. The uncorrected (top) and corrected (bottom) matrix of x-ray intensities are shown in figure 1. The final spectra were created by adding the intensities along each column; therefore the line

**Figure 1.** Spectral data before (top panel) and after (bottom panel) curvature straightening.

broadening produced by the curvature is greatly reduced after the correction.

Each spectrum was fit with Gaussian functions for the individual peaks and a third order polynomial function for the background. During the fit each data point was weighted by their statistical uncertainty. In order to achieve lower uncertainties for the line positions, spectra measured at 3.87 and 7.91 keV beam energies were added and fit. The peak positions from the summed spectrum were used as constraints when fitting the spectrum at each beam energy and peak widths were constrained to be equal.

The two spectrometers were self calibrated using the well known energies of the He-like w , x , y , z lines [41], and Li-like q and r lines [42], where these are labeled according to Gabriel [8]. To take into account differences in detector efficiencies and geometrical orientations with respect to the EBIT plasma, horizontal and vertical spectra were normalized to each other using the fundamentally unpolarized Li-like m line recorded at an electron beam resonance energy of 2.25 keV. This transition $1s^2 2p_{3/2}^2 P_{3/2} - 1s 2p^2(^1S) ^2S_{1/2}$ is unpolarized due to the axial symmetry of the $J = 1/2$ excited states (see, e.g. [1]). The $1s^2 2s ^2S_{1/2} - 1s 2s 2p(^3P) ^2P_{1/2}$ (r) transition is also intrinsically unpolarized and observed in our He-like measured spectra at 3.87 keV; however it is very weak and blended with q line, so was not included in the analysis. From the ratio of the m line intensities in the two spectrometer orientations, we found that the horizontal orientation is about 1.46 times more efficient than the vertical, in agreement with Henderson *et al* [6] and Takacs *et al* [16]. The fact that the experimental efficiency of the horizontal and the vertical spectrometers is so close to each other is indication that the two spectrometers observe mostly the same region of the EBIT plasma and with that we can assume similar plasma conditions.

The measured spectra observed with the horizontal and vertical crystal spectrometers at a beam energy of 3.87 and

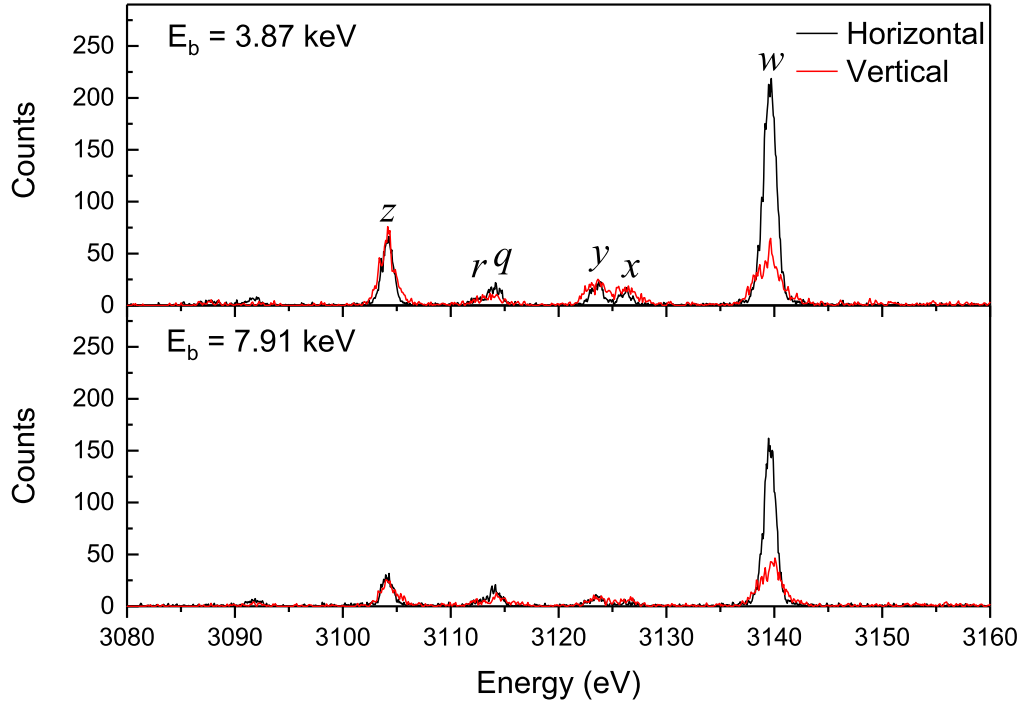


Figure 2. Measured spectra from the horizontal (black) and vertically (red) oriented spectrometers. (Top) Measured spectra at an electron beam energy setting of 3.87 keV. (Bottom) Spectra at a beam energy of 7.91 keV.

7.91 keV are shown in the figure 2, where the vertical spectra have been normalized to the horizontal. This figure shows that the spectral features from the vertically oriented spectrometer are slightly broader due to the extended source size previously mentioned. From the Gaussian fits to individual peaks, we found that the horizontal spectrometer produces a FWHM of about 1.4 eV, while the vertical has a FWHM of about 2.3 eV.

3.2. Calculating experimental polarization

The polarization of emitted x-rays from the EBIT plasma specify the direction of the electric field vector of the electromagnetic wave. The polarization and angle of observation are defined with respect to the quantization axis, which is same as the direction of the electron beam. All measurements were taken at an observation angle of 90° relative to the quantization axis, and we use the following definition of the linear polarization, P :

$$P = \frac{I_{\parallel} - I_{\perp}}{I_{\parallel} + I_{\perp}}, \quad (1)$$

where I_{\parallel} and I_{\perp} are the intensities of the light with the electric field vectors parallel and perpendicular to the direction of the beam, respectively.

The crystal spectrometers are sensitive to the polarization of the incoming x-ray photons and their measured intensities are defined as

$$I^{obs} = R_{\parallel} I_{\parallel} + R_{\perp} I_{\perp}, \quad (2)$$

where R_{\parallel} and R_{\perp} are the crystal reflectivities for light polarized parallel and perpendicular to the crystal's plane of dispersion (not with respect to the quantization axis as I_{\parallel} and I_{\perp} are defined), respectively. The parallel and perpendicular

reflectivity components are non-equal, and sensitive to the Bragg angle. Using the relative reflectivity, defined as $R = R_{\parallel}/R_{\perp}$, we can write the observed horizontal (I_H) and vertical (I_V) spectral intensities as:

$$I_H = I_{\parallel} + R I_{\perp}, \quad (3)$$

$$I_V = R I_{\parallel} + I_{\perp}. \quad (4)$$

For perfect crystals, reflectivity (R) values vary as $\cos^2(2\theta)$, while mosaic crystals vary as $|\cos(2\theta)|$ [43], where θ is the Bragg angle proportional to the photon energy. Real crystal reflectivities are typically in between these values and must be considered for the appropriate Bragg angles. Reflectivity values for the Si(111) crystals used in this work were calculated using x-ray Optics utilities (XOP) [44] for a range of photon energies as shown in figure 3. These values are consistent with values provided by Henke *et al* [45], commonly used to estimate R .

By combining equations (1), (3), and (4), the linear polarization of our experimental setup can be expressed as:

$$P = \left(\frac{1 + R}{1 - R} \right) \left(\frac{I_H - I_V}{I_H + I_V} \right), \quad (5)$$

where I_V is normalized to I_H to remove any differences in efficiency and geometry, as previously discussed. Final uncertainties include contributions from fitting, normalization, and the statistical uncertainty. While all of the aforementioned sources contributed to the final uncertainty, the statistical uncertainty was predominant. The spiraling motion of the electrons in the field of the superconducting magnet of the EBIT, discussed in section 5 can systematically reduce the polarization and was also taken into account.

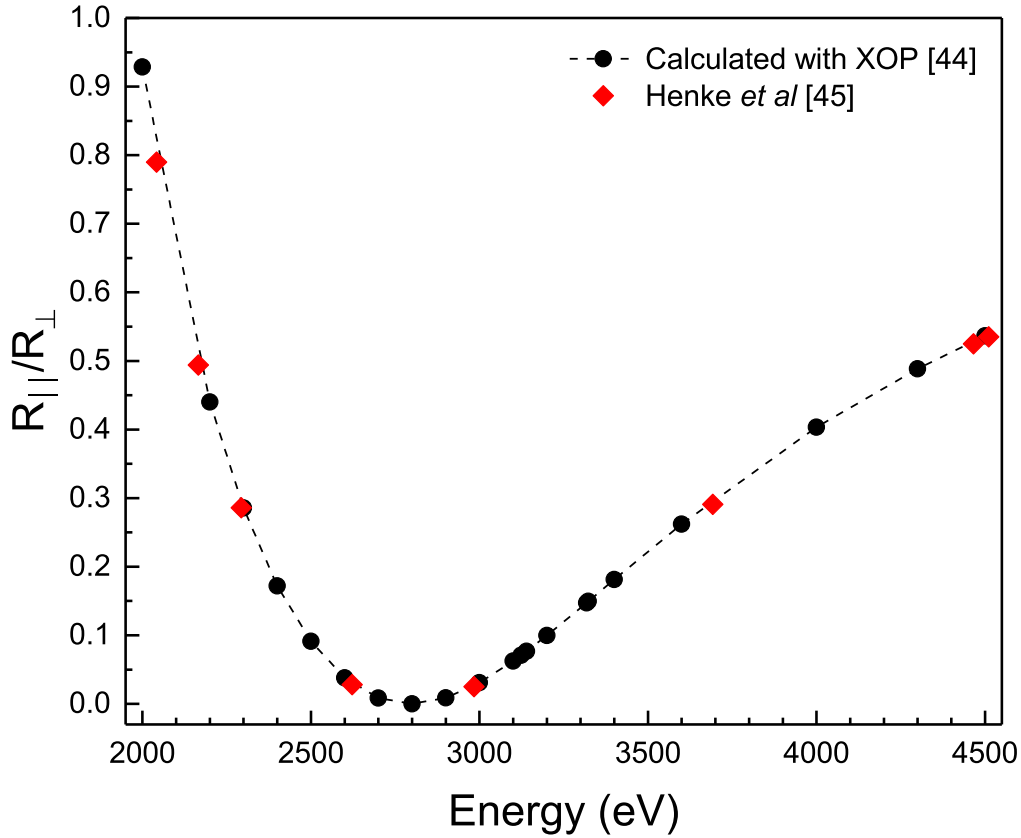


Figure 3. Reflectivity ratio calculated as a function of incident photon energy (Bragg angle) for a Si(111) crystal. Black circles show R values calculated using XOP [44]. Red diamonds show R values from Henke *et al* [45].

4. Theoretical approach

The analysis of the polarization of x-ray emission in highly-charged Ar ions was based on the CR modeling of the EBIT plasma using the NOMAD code [30]. The CR simulations were performed with magnetic sublevel atomic kinetics in steady state representing the current experimental conditions. Atomic processes such as radiative decay, excitation (de-excitation), ionization (3-body recombination), autoionization (AI), dielectronic capture and RR were considered in our model. The corresponding cross sections and probabilities were calculated using the FAC code [31], however the obtained radiative transition probabilities and RR cross sections were not sublevel-resolved. Nonetheless, the radiative transition probabilities for magnetic sublevels can be derived from their corresponding total rates using the Wigner–Eckart theorem [16]. As for the RR, the cross sections were distributed evenly in the magnetic sublevels. The validation of this approximation will be discussed in section 5.2 as RR can create alignment in magnetic sublevels [46, 47].

Our CR model includes configurations with single electron excitation up to principal quantum number (n) 5, and autoionizing states with single K-shell electron excitation to $n = 3$ for H-like to Be-like ions, resulting in about 2500 magnetic sublevels. Electric-dipole allowed (E1) transitions within all configurations, forbidden (M1, E2, and M2) transitions for configurations with single electron excitation up to

$n = 3$, and the two-photon decay $1s^2 \ ^1S_0 - 1s2s \ ^1S_0$ (2E1) transition [48] were accounted for. Using this atomic data, NOMAD calculated the rate coefficients for the Gaussian EEDF with FWHM of 40 eV at an electron density $n_e = 10^{11} \text{ cm}^{-3}$ and solved a set of rate equations to determine the magnetic sublevel populations.

The intensities of each spectral line associated with electric field vector polarized parallel and perpendicular to the beam direction were calculated using the following equation [20]:

$$I_{||,\perp} \propto \Delta E \sum_{M_f=-J_f}^{J_f} N(M_f) \times \sum_{M_i=-J_i}^{J_i} M_{I_{||,\perp}}(\Delta M, \theta) A(J_i M_i - J_f M_f). \quad (6)$$

Here ΔE is the transition energy, $N(M_f)$ is the population of the upper level with magnetic quantum number M_f , and $A(J_i M_i - J_f M_f)$ represents the magnetic sublevel radiative transition probabilities. $M_{I_{||,\perp}}(\Delta M, \theta)$ denotes the relative multipole intensities where ΔM is the absolute difference in magnetic quantum numbers of lower and upper levels, and θ is the angle between the quantization axis (direction of the electron beam) and the direction of observation ($\theta = 90^\circ$ in our case). The summation in equation (6) is carried out over the J_f components to obtain the total intensity of each spectral line as energy levels are degenerate over magnetic quantum numbers in the absence of any external fields. The values of relative multipole intensities for dipole (E1, M1) and quadrupole (E2, M2) transitions were taken from [20]. The intensities calculated for the parallel and perpendicular polarization modes were used

Table 2. Summary of results on linear polarization of He-like transitions. Transitions labeled as done by Gabriel [8]. Line energy in eV from Saloman [36, 41].

Beam energy	Key	Transition	E (eV)	$P_{Exp.}(90^\circ \pm \gamma)$	P_{Theory} (Excitation + Radiative)						NOMAD _{FULL}	
					No cascades		Cascades		No 2-photon		90°	$90^\circ \pm \gamma$
					90°	$90^\circ \pm \gamma$	90°	$90^\circ \pm \gamma$	90°	$90^\circ \pm \gamma$		
3.87 keV	w	$1s^2\ ^1S_0 - 1s2p\ ^1P_1$	3139.58	0.54 ± 0.07	0.60	0.59	0.58	0.56	0.52	0.50	0.58	0.56
	x	$1s^2\ ^1S_0 - 1s2p\ ^3P_2$	3126.23	-0.42 ± 0.10	-0.52	-0.47	-0.50	-0.46	-0.50	-0.46	-0.50	-0.46
	y	$1s^2\ ^1S_0 - 1s2p\ ^3P_1$	3123.53	-0.32 ± 0.10	-0.37	-0.34	-0.30	-0.28	-0.15	-0.14	-0.30	-0.28
	z	$1s^2\ ^1S_0 - 1s2s\ ^3S_1$	3104.15	-0.14 ± 0.09	0.00	0.00	-0.15	-0.14	-0.15	-0.14	-0.15	-0.14
7.91 keV	w	$1s^2\ ^1S_0 - 1s2p\ ^1P_1$	3139.58	0.44 ± 0.08	0.47	0.47	0.46	0.45	0.46	0.45	0.40	0.40
	x	$1s^2\ ^1S_0 - 1s2p\ ^3P_2$	3126.23	-0.45 ± 0.19	-0.47	-0.45	-0.44	-0.43	-0.43	-0.41	-0.052	-0.049
	y	$1s^2\ ^1S_0 - 1s2p\ ^3P_1$	3123.53	-0.05 ± 0.15	0.036	0.034	0.053	0.052	0.010	0.010	0.012	0.012
	z	$1s^2\ ^1S_0 - 1s2s\ ^3S_1$	3104.15	-0.08 ± 0.10	0.00	0.00	-0.047	-0.046	-0.047	-0.046	-0.023	-0.022

in equation (1) to determine the polarization of x-ray lines listed in table 2.

To address the effect of cascades on the polarization of $1s^2-1s2l$ lines in He-like Ar ions, we also performed calculations that included only two levels involved in the transition (the ground state and the upper level). Here, the upper magnetic sublevels are only populated by direct electron-impact excitation from the ground state and depopulated via radiative decay. Therefore, the population of magnetic sublevels in this coronal approximation is calculated through

$$N(M_f) = \frac{N(1s^2)n_e C_{gs \rightarrow M_f}}{A(J_i M_i - J_f M_f)} \quad (7)$$

with $C_{gs \rightarrow M_f}$ representing the electron-impact excitation rate coefficients from the ground state. The results of this 2-level model are also presented in table 2 under the ‘No cascades’ column.

5. Results and discussion

In table 2, the measured and theoretical polarizations of the four $1s^2-1s2l$ lines in He-like Ar¹⁶⁺ ion are listed at the beam energies of 3.87 and 7.91 keV. The measured positive value of polarization for the resonance line (w) suggests that it is polarized parallel to the quantization axis while the forbidden (z and x) and intercombination (y) lines are polarized in a direction perpendicular to the quantization axis. The positive degree of polarization of resonance line (w) can also be interpreted through the relative difference of intensities in the horizontal and vertical spectra (figure 2) using equation (5). Polarization of the satellite line $1s^22s^2S_{1/2} - 1s2s2p(^3P)^2P_{3/2}$ (q) observed in the measured spectra is not listed in the table as its uncertainty is large due to blending with the unpolarized r satellite, and will be included in a later polarization study of DR lines with better statistics.

Because of the transverse thermal energy component of the electron beam in the EBIT, the observation angle is slightly off from the assumed value of 90° by an angle, called pitch angle [14, 16]. This angle can be calculated using the theory of [49] which states that the product of the beam area and the transverse temperature is a constant. Given a maximum beam radius at the cathode of the $r_c = 1.5$ mm, the electron beam radius at the trap $r_t = 35$ μm [50], and an electron gun temperature $T = 1400$ K, the transverse energy component of the electron beam, E_\perp can be estimated by:

$$E_\perp = kT \left(\frac{r_c^2}{r_t^2} \right) = 222 \text{ eV} \quad (8)$$

and the resultant pitch angle is

$$\gamma = \sin^{-1} \left(\sqrt{\frac{E_\perp}{E_{beam}}} \right) = 13.9^\circ \quad (9)$$

for the 3.87 keV beam energy. The transverse energy component is independent of the electron beam energy according to equation (8), however at 7.91 keV beam energy the pitch angle becomes 9.6°. Using the methods described by Gu *et al*

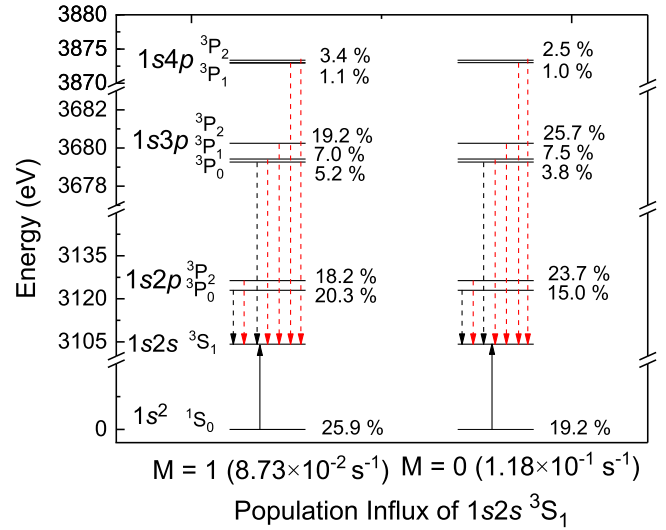


Figure 4. Population influx (population × rates) for the $1s2s^3S_1$ sublevels with magnetic quantum numbers 1 and 0 at the electron beam energy of 3.87 keV. Populations of magnetic sublevels are normalized to 1.

[51], we can calculate the ‘true’ polarization ($P_{Exp.}(90^\circ)$ for pitch angle of zero) as:

$$P_{Exp.}(90^\circ) = \frac{2P}{2 - \sin^2 \gamma (3 \pm P)}, \quad (10)$$

where (−) is used for electric dipole transitions and (+) for magnetic dipole transitions [51]. The angular distribution of magnetic quadrupole transition x behaves like that for E1 transitions, so negative sign is used in equation (10) to obtain its polarization at 90°. Plugging in 222 eV for E_\perp , P values from table 2, and 3.87 keV for E_{beam} , the estimated polarization values at an observation angle of 90° are: $P_w = 0.58$, $P_x = -0.46$, $P_y = -0.36$, and $P_z = -0.15$ at 3.87 keV. At 7.91 keV the estimated $P_{exp}(90^\circ)$ values are: $P_w = 0.45$, $P_x = -0.48$, $P_y = -0.05$, and $P_z = -0.08$. These values, shown in table 2 with the measured values $P_{Exp.}(90^\circ \pm \gamma)$, fall within the experimental uncertainty.

The ‘No Cascades’ column in table 2 refers to the polarization calculated using 2-level model, which included only excitation from the ground state of the He-like ion. Results under column ‘Cascades’ in the same table include the electron-impact excitation and radiative cascades within the considered configurations of the He-like Ar¹⁶⁺ ion. The comparison of the two results reflects the contribution of radiative cascades on the polarizations of $1s^2-1s2l$ lines. The most significant contribution of cascades is observed for the z line which is unpolarized in the 2-level model due to isotropic excitation from the ground state. To clarify the radiative cascade effects on the polarization of this line, the population kinetics for the magnetic sublevels of the upper level $1s2s^3S_1$ is shown in the figure 4 at beam electron energy of 3.87 keV. The population of magnetic sublevels with $|M| = 1$ are equal due to axial symmetry.

The population influx (population × rates) of sublevels with magnetic quantum numbers 1 and 0 are $8.73 \times 10^{-2} \text{ s}^{-1}$ and $1.18 \times 10^{-1} \text{ s}^{-1}$ respectively, at an electron energy of

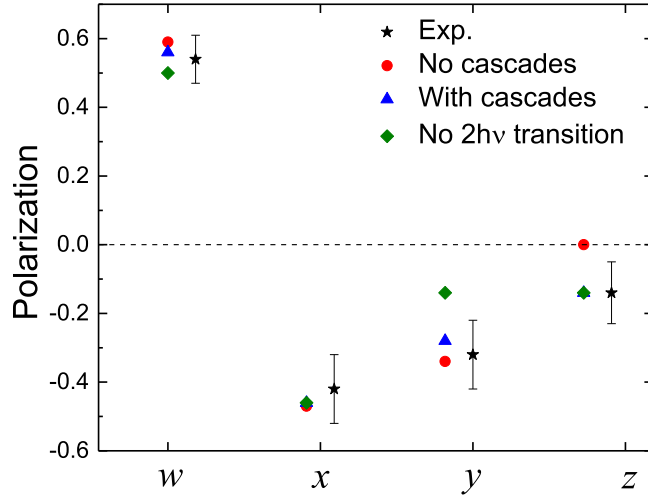


Figure 5. Comparison of measured and theoretical polarizations of $1s^2 - 1s2l$ lines at the electron beam energy of 3.87 keV for pitch angle of 13.9° . ‘No cascades’ represents the 2-level model results, while ‘Cascades’ includes the electron-impact excitation and radiative cascades within He-like Ar^{16+} ion. ‘No $2h\nu$ transition’ excludes only two-photon transition $1s^2 \ ^1S_0 - 1s2s \ ^1S_0$ from the model including cascades. Error bars represent the uncertainties in the experimental polarizations.

3.87 keV. In figure 4, black lines represent the isotropic population transfer from 1S_0 , 3P_0 levels while the red lines refer to the alignment created by $^3P_{1,2}$ in 3S_1 magnetic levels. Radiative cascade contributions to the populations of magnetic sublevels of 3S_1 with M equals 1 and 0 amounts to about 74% and 81% respectively. Both $1s3l$ and $1s4l$ levels are open for direct excitation from the ground state as their threshold energies are about 3.68 keV and 3.87 keV respectively. The contribution of $1s2l$, $1s3l$, and $1s4l$ levels through radiative decays to $1s2s$ (3S_1 $M = 0$) are about 39%, 37% and 5%. Thus, the direct excitation from the ground state is insufficient to explain the polarization of the z line even if the cross sections are anisotropic as predicted by relativistic calculations [20, 52]. The calculated polarization value of -0.14 is in excellent agreement with the measured value of -0.14 ± 0.09 at an observation angle of $90^\circ \pm \gamma$. Lines w , x and y show very small contribution of radiative cascades at 3.87 keV and the two calculations agree with the measured values within the experimental uncertainties (see figure 5).

As the beam energy increases to 7.91 keV, high $1snl$ states are open for direct excitation from the ground state. Cascades from $n > 5$ will not be important and are not considered in our model. This is indeed confirmed as the polarizations of $1s^2 - 1s2l$ lines did not change by excluding $n = 5$ levels from the model. The theoretical results including the radiative cascades are in very good agreement with the measured polarization values.

5.1. Two-photon transition $1s^2 \ ^1S_0 - 1s2s \ ^1S_0$ and polarization

A single-photon radiative decay from the upper level $1s2s \ ^1S_0$ to the ground state $1s^2 \ ^1S_0$ is forbidden due to selection rules. However, this level can decay into the ground state by

simultaneous emission of two E1 photons with a transition rate of about $4.2 \times 10^8 \text{ s}^{-1}$ [48]. In He-like Ar, the $1s2s \ ^1S_0$ level can also decay radiatively to the $1s2s \ ^3S_1$ level by an M1 transition, and to the $1s2p \ ^3P_1$ level by a spin-forbidden E1 transition. The transition rates of these M1 and E1 transitions are 6.53 s^{-1} and $1.44 \times 10^2 \text{ s}^{-1}$ respectively, which are several orders of magnitude smaller than that of the 2E1 transition. Therefore, neglecting this strong two-photon transition in CR modeling should result in a significant overpopulation of the $1s2s \ ^1S_0$ level that may affect the other $1s2l$ levels and thus the calculated values of polarizations.

This conclusion is indeed confirmed by comparison of the results with and without the 2E1 transition. The ‘No 2-photon’ column in table 2 that corresponds to the latter case shows that the linear polarization values of the resonance and intercombination lines decrease by about 10% and 50%, respectively for the 3.87 keV electron beam energy, while the forbidden lines x and z do not undergo any noticeable change. The upper levels of the x and z transitions are connected with the 2^1S_0 level via very weak excitation ($\Delta J = 2$) and radiative (M1 with a small transition energy) processes, and therefore overpopulation of the 2^1S_0 level does not result in changes in their polarizations. However, both the optically-allowed excitation $2^1S_0 - 2^1P_1$ and the intercombination radiative decay $2^1S_0 - 2^3P_1$ are highly effective in transferring population into the upper levels of w and y lines and this results in significant changes of their polarizations. For example, without the 2E1 process the magnetic sublevels of 3P_1 with $M = 1$ and 0 receive about 41% and 56% of their total population influx directly from the decay of the 2^1S_0 level. This strong isotropic emission from 2^1S_0 to 3P_1 destroys the alignment created in the magnetic sublevels and the polarization of the intercombination line increases from -0.28 to -0.14 . Note that the former value (with the inclusion of 2E1 transition) is in excellent agreement with the measured polarization of -0.32 ± 0.10 at an observation angle of $90^\circ \pm \gamma$.

Observed agreement of the theoretical and measured values illustrates the critical importance of considering 2E1 transition from 2^1S_0 for the polarizations of $1s^2 - 1s2l$ lines for low-density EBIT plasma. Intensity ratios of resonance, intercombination and forbidden lines in He-like ions are often used for the diagnostics of astrophysical and laboratory plasmas and most of the studies have ignored the two-photon transition from 2^1S_0 in the analysis. The 2E1 decay from 2^1S_0 to the ground level is the dominating decay channel along the isoelectronic sequence. Radiative decay rates of the single photon M1 and spin-forbidden E1 transitions from the same level are several orders smaller than the 2E1 decay for He-like ions along the whole isoelectronic sequence and hence, these transitions will not play any role for the population kinetics of 2^1S_0 level. Therefore, this strong two-photon transition should be taken into account for all Z as it can effect significantly the polarizations of resonance and intercombination lines as well as the corresponding intensity ratios, particularly for low-density plasmas.

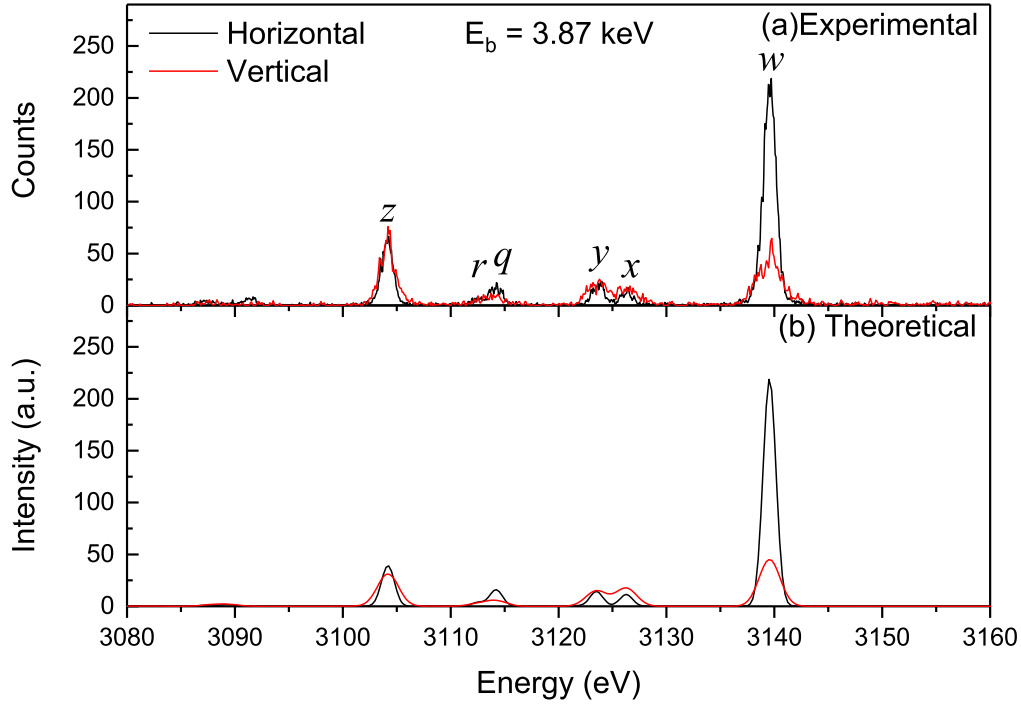


Figure 6. (a) X-ray emission spectra recorded by horizontal (black curve) and vertical (red curve) crystal spectrometers for w , x , y and z lines in He-like and satellite lines q and r in Li-like Ar ions at electron beam energy of 3.87 keV; (b) simulated spectra with NOMAD by taking into account of charge exchange.

5.2. RR and CX

RR of multiply charged ions and CX with the neutral atoms inside the trap shift the ionization balance to lower stages. DR is not important for the present experimental conditions due to its resonance nature while 3-body recombination is negligible due to low density of the EBIT plasma. For the electron energy below the ionization potential of He-like Ar¹⁶⁺ ion (4.12 keV), only collisional excitation and radiative cascades contribute to the population flux into $1s2l$ levels. Thus, there is no effect of recombination on the polarizations of $1s^2 - 1s2l$ lines at 3.87 keV. However, as the beam energy increases to 7.91 keV, recombination from H-like ions can modify the populations of $1s2l$ levels in He-like Ar ions and consequently, the polarization of lines may change.

The calculated RR cross sections σ_{RR} are on the order of 10^{-24} cm² for the beam energies of interest and the corresponding rates are estimated to be about $(10^{-3}$ to $10^{-5})$ s⁻¹ using the product $\sigma_{RR}v n_e$ where n_e and v are electron density and velocity, respectively. The CX cross sections for an ion with the charge Z can be obtained from classical-trajectory Monte-Carlo estimates [53] to be $\sigma_{CX} \approx Z \times 10^{-15}$ cm². Since the neutral density N_N and the relative velocity of the neutral atoms and ions v_R inside EBIT is unknown, it enters the CR model as a free parameter. The fitting of measured line intensity ratios of Li-like and He-like Ar ions with the simulated spectra provided an estimate of $N_N v_R \approx 3 \times 10^{13}$ cm⁻² s⁻¹ at $E_b = 3.87$ keV. The CX rate comes out to be on the order of 0.5 s⁻¹ which is substantially larger than the RR rates summed over all channels. Therefore, we can conclude that the effect of RR on the populations of $1s2l$ levels is small as compared to CX recombination.

In order to visually compare with the experimental observations, $I_{||}$ and I_{\perp} calculated from the complete model along with crystal reflectivities were used in equations (3) and (4) to obtain the theoretical horizontal and vertical spectra. The calculated horizontal and vertical spectra were convolved with Gaussian functions with 1.4 eV and 2.3 eV FWHM values, respectively. As shown in figure 6, the measured and simulated spectra show good agreements.

The well-known scaling $n_{CX} = Z^{0.75}$ [54] for the principal quantum number of the dominantly populated initial levels due to CX provides $n_{CX} = 9$ for our case. However, our CR model only includes states up to $n = 5$ and therefore some approximations were made to analyze the initial state-dependence of the CX process. It is also known that at high-collision energies the l -dependence of CX cross sections is close to statistical while at low energies it may deviate from the $2l + 1$ distribution [55]. Hence, to test the effect of l -distributions on line polarizations we performed two calculations in which CX process was exclusively redirected into the $1s5l$ states. In the first one, the CX cross sections were distributed according to $2l + 1$ while in the other, the cross sections into different $1s5l$ states were independent of l . It was found that the polarizations of the $1s^2 - 1s2l$ lines do not change noticeably between the two cases. For example, polarization of the x line is -0.052 and -0.065 for the statistical and equal population distribution over $1s5l$ states, respectively. The results with the complete model by including statistically-distributed CX and RR are presented in the last column 'NOMAD_{FULL}' of table 2. It was found that CX affects the polarizations of $1s^2 - 1s2l$ lines, and in particular, the x line at $E_b = 7.91$ keV. The theoretical

polarizations (with and without CX) of the w , y , and z lines agree with the measured values within the experimental uncertainties. However, the forbidden line x is weakly polarized in the complete model and lies outside the experimental uncertainty limit. This line is rather faint in the measured spectra (figure 2(b)), therefore we plan explore this further in future studies including the measurements of x-ray emission following CX recombination.

The uncertainty in theoretical calculations at 3.87 keV is primarily due to the excitation cross sections (known to within 10%–20%) and radiative transition probabilities (<5%). Therefore, the estimated uncertainty of the calculated polarizations at this energy can be fairly taken to be within 20%. As the beam energy is increased above the ionization energy of He-like Ar ions, the CX recombination from H-like to He-like ion provides additional and not well defined uncertainty. As discussed earlier, the unknown CX contribution is included by making several assumptions in the present case which can only be elucidated through additional experimental verification as well as reasonably accurate calculations of CX cross sections. Therefore, the uncertainties are relatively higher at 7.87 keV as compared to 3.87 keV beam energy.

6. Conclusions

We have presented the study of the linear polarization of dominant x-ray transitions in He-like Ar ions both experimentally and theoretically. X-ray emission, produced by a monoenergetic electron beam at the NIST EBIT, was measured with two polarization sensitive Johann-type crystal spectrometers at an electron beam energy of 3.87 and 7.91 keV. Due to depolarization effects from the spiral motion of the electrons, the measured polarizations of the $1s^2 - 1s2l$ lines were slightly smaller than the estimated true values. The corrected calculated values however all fell within the experimental uncertainties.

Our theoretical results based on the CR modeling of magnetic sublevels are in good agreement with the measured values. Detailed analysis of the theoretical predictions revealed that radiative cascades have strong contribution on the polarization of $1s^2 - 1s2l$ transitions at these energies. It was found that the polarizations of the resonance (w) and intercombination (y) lines are reduced significantly without including the two-photon transition ($1s^2\ ^1S_0 - 1s2s\ ^1S_0$) in the model. In addition, the effects of the CX recombination on the polarizations of the four He-like lines were investigated qualitatively.

Acknowledgments

This work was partially supported by the NIST Measurement Science and Engineering (MSE) Research Grant (#70NANB18H282 and #70NANB19H024), the National Science Foundation (#1806494), and by NASA/GSFC (#80NSSC18K0234). Author C I Szabo performed this work

with financial assistance from U.S. Department of Commerce, NIST (# 70NANB15H051).


ORCID iDs

Dipti  <https://orcid.org/0000-0001-6675-8509>

A C Gall  <https://orcid.org/0000-0002-8260-2229>

C I Szabo  <https://orcid.org/0000-0002-6125-7948>

E Takacs  <https://orcid.org/0000-0002-2427-5362>

Yu Ralchenko  <https://orcid.org/0000-0003-0083-9554>

References

- [1] Inal M K and Dubau J 1987 *J. Phys. B: At. Mol. Opt. Phys.* **20** 4221–39
- [2] Haug E 1972 *Sol. Phys.* **25** 425
- [3] Weisskopf M C, Elsner R F, Kaspi V M, O'dell S L, Pavlov G G and Ramsey B D 2009 X-ray polarimetry and its potential use for understanding neutron stars *Neutron Stars and Pulsars* ed W Becker (Berlin: Springer) p 589
- [4] Zanardo G, Staveley-Smith L, Gaensler B M, Indebetouw R, Ng C Y, Matsuura M and Tzioumis A K 2018 *Astrophys. J.* **861** L9
- [5] Kieffer J C, Matte J P, Chaker M, Beaudoin Y, Chien C Y, Coe S, Mourou G, Dubau J and Inal M K 1993 *Phys. Rev. E* **48** 4648–58
- [6] Henderson J R *et al* 1990 *Phys. Rev. Lett.* **65** 705–8
- [7] Smith A J, Beiersdorfer P, Wong K L and Reed K J 2001 Measurement of the polarization of the $K_{\beta 2}$ line of helium-like V^{21+} *3rd US-Japan Plasma Polarization Spectroscopy Workshop (Livermore, CA)* 299
- [8] Gabriel A H 1972 *Mon. Not. R. Astron. Soc.* **160** 99–119
- [9] Beiersdorfer P, Brown G, Utter S, Neill P, Reed K J, Smith A J and Thoe R S 1999 *Phys. Rev. A* **60** 4156–9
- [10] Beiersdorfer P *et al* 1996 *Phys. Rev. A* **53** 3974–81
- [11] Beiersdorfer P, López-Urrutia J C, Decaux V, Widmann K and Neill P 1997 *Rev. Sci. Instrum.* **68** 1073–6
- [12] Nakamura N, Kato D, Miura N, Nakahara T and Ohtani S 2001 *Phys. Rev. A* **63** 024501
- [13] Robbins D L *et al* 2006 *Phys. Rev. A* **74** 022713
- [14] Beiersdorfer P and Slater M 2002 *Phys. Rev. E* **64** 066408
- [15] Robbins D L, Faenov A Y, Pikuz T A, Chen H, Beiersdorfer P, May M J, Dunn J, Reed K J and Smith A J 2004 *Phys. Rev. A* **70** 022715
- [16] Takacs E *et al* 1996 *Phys. Rev. A* **54** 1342–50
- [17] Weinheimer J, Ahmad I, Herzog O, Kunze H J, Bertschinger G, Biel W, Borchert G and Bitter M 2001 *Rev. Sci. Instrum.* **72** 2566
- [18] Shi J, Xiao S, Qian J, Huang X and Cai H 2010 *Nucl. Instrum. Methods Phys. Res. A* **624** 137–40
- [19] Hake P, Mancini R C, Gauthier J C, Mínguez E, Dubau J and Cornille M 2004 *Phys. Rev. E* **69** 056405
- [20] Hake P, Mancini R C, Harris C, Neill P, Beiersdorfer P, Csanak G and Zhang H L 2007 *Phys. Rev. A* **76** 012716
- [21] Reed K J and Chen M H 1993 *Phys. Rev. A* **48** 3644
- [22] Fontes C J, Zhang H L and Samson D H 1999 *Phys. Rev. A* **59** 295
- [23] Jun J, Chen-Zhong D and Lu-You X 2014 *Chin. Phys. Lett.* **31** 023401
- [24] Chen Z B, Dong C Z, Xie L Y and Jiang J 2014 *Phys. Rev. A* **90** 012703
- [25] Chen Z B and Zeng J L 2015 *J. Phys. B: At. Mol. Opt. Phys.* **48** 245201
- [26] Chen Z 2018 *Phys. Plasmas* **25** 052105

- [27] Bostock C J, Fursa D V and Bray I 2009 *Phys. Rev. A* **80** 052708
- [28] Kai T, Nakazaki S and Berrington K A 2005 *Nucl. Instrum. Methods Phys. Res. B* **235** 249–51
- [29] Surzhykov A, Litvinov Y, Stöhlker T and Fritzsche S 2013 *Phys. Rev. A* **87** 052507
- [30] Ralchenko Yu and Maron Y 2001 *J. Quant. Spectr. Rad. Transf.* **71** 609–21
- [31] Gu M F 2008 *Can. J. Phys.* **86** 675–89
- [32] Gillaspy J, Roberts J, Brown C and Feldman U 1993 *6th Int. Conf. on the Physics of Highly Charged Ions* 274, p 682
- [33] Fahy K, Sokell E, O’Sullivan G, Aguilar A, Pomeroy J M, Tan J N and Gillaspy J D 2007 *Phys. Rev. A* **75** 032520
- [34] Holland G E, Boyer C N, Seely J F, Tan J N, Pomeroy J M and Gillaspy J D 2005 *Rev. Sci. Instrum.* **76** 073304
- [35] Porto J V, Kink I and Gillaspy J D 2000 *Rev. Sci. Instrum.* **71** 3050–8
- [36] Kramida A, Ralchenko Y, Reader J and NIST ASD Team 2018 NIST Atomic Spectra Database (ver. 5.6.1), (<https://physics.nist.gov/asd>) [25 July 2019] National Institute of Standards and Technology, Gaithersburg, MD
- [37] Kessler E G, Szabo-Foster C I, Cline J P, Henins A, Hudson L T, Mendenhall M H and Vaudin M D 2017 *J. Res. Natl Inst. Stand. Technol.* **122** 1
- [38] Hudson L *et al* 2007 *Nucl. Instrum. Methods Phys. Res. A* **580** 33–6
- [39] Brennan S, Cowan P L, Deslattes R D, Henins A, Lindle D W and Karlin B A 1989 *Rev. Sci. Instrum.* **60** 2243–6
- [40] Zschornack G, Müller G and Musiol G 1982 *Nucl. Instrum. Methods Phys. Res.* **200** 481–90
- [41] Saloman E B 2010 *J. Phys. Chem. Ref. Data* **39** 033101
- [42] Yerokhin V A and Surzhykov A 2018 *J. Phys. Chem. Ref. Data* **47** 023105
- [43] Burek A 1976 *Space Sci. Instrum.* **2** 53–104
- [44] Dejus R J and Sanchez del Rio M 1996 *Rev. Sci. Instrum.* **67** 3356
- [45] Henke B, Gullikson E and Davis J 1993 *At. Data Nucl. Data Tables* **54** 181–342
- [46] Scofield J H 1991 *Phys. Rev. A* **44** 139
- [47] Bettadj L, Inal M K, Surzhykov A and Fritzsche S 2010 *Nucl. Instrum. Methods Phys. Res. B* **268** 3509–16
- [48] Drake G W F 1986 *Phys. Rev. A* **34** 2871–80
- [49] Herrmann G 1958 *J. Appl. Phys.* **29** 127–36
- [50] Levine M *et al* 1989 *Nucl. Instrum. Methods Phys. Res. B* **43** 431–40
- [51] Gu M F, Savin D W and Beiersdorfer P 1999 *J. Phys. B: At. Mol. Opt. Phys.* **32** 5371–8
- [52] Zhang H L, Sampson D H and Clark R E H 1990 *Phys. Rev. A* **41** 198
- [53] Otranto S, Olson R E and Beiersdorfer P 2006 *Phys. Rev. A* **73** 022723
- [54] Olson R E 1981 *Phys. Rev. A* **24** 1726
- [55] Beiersdorfer P, Olson R E, Brown G V, Chen H, Harris C L, Neill P A, Schweikhard L, Utter S B and Widmann K 2000 *Phys. Rev. Lett.* **85** 5090–3